Journal of Materials Chemistry A

Accepted Manuscript

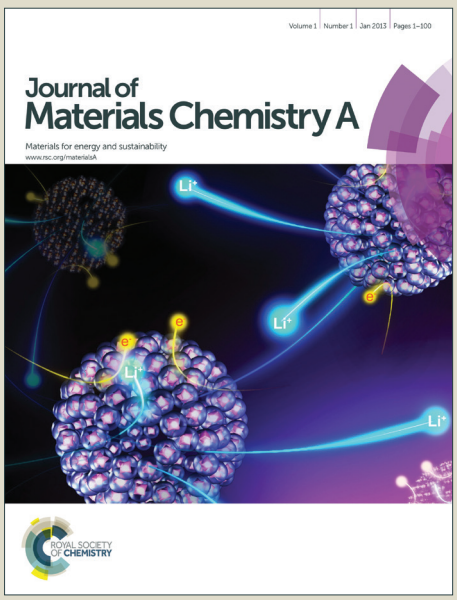

ROYAL SOCIETY OF CHEMISTRY

www.rsc.org/materialsA

Cite this: DOI: 10.1039/c0xx00000x

www.rsc.org/xxxxxx

ARTICLE TYPE

High Capacitive Performance of Exfoliated Biochar Nanosheets from Biomass Waste Corn Cob

Matthew Genovese[a], Junhua Jiang[b,*], Keryn Lian[a,], Nancy Holm[b]**

Received (in XXX, XXX) Xth XXXXXXXXX 20XX, Accepted Xth XXXXXXXXX 20XX

DOI: 10.1039/b000000x

A high performance exfoliated biochar carbon with a layered nanosheet structure was prepared from a low cost agricultural residue (corn cob) via a novel synthesis strategy involving biomass pre-treatment, nitrogen pyrolysis, and a high temperature thermal-chemical flash exfoliation. The exfoliation strategy resulted in porous carbon nanosheets with BET specific surface area of 543.7 m^2 g^{-1}, far higher than the 7.9 m^2 g^{-1} of the natural biochar produced without any pre- or post-treatment modifications. The exfoliated material also showed increased oxygen functionality in the form of electrochemically active quinone and pyrone surface groups. This combination of high specific surface area and highly active surface functional groups resulted in very promising capacitive performance, demonstrating a high capacitance of 221 F g^{-1}, over 100 times greater than the natural biochar. The exfoliated biochar electrodes fabricated without any conductive additives showed outstanding high rate capability retaining 78 % of their low rate capacitance at a fast 40 A g^{-1} discharge. This combination of high capacitance and fast charge-discharge capability distinguishes this material from most other high surface area activated carbons; in fact, the electrochemical behaviour more closely resembles that of designer nanomaterials such as graphene and carbon nanotubes. The biochar electrodes were also extremely durable showing only a 3 % reduction in capacitance after 5000 successive potential cycles. The exfoliation strategy developed here could provide a novel route for the low cost production of high performance energy storage materials from a variety of waste biomass feedstocks.

Introduction

The availability of robust, low-cost energy storage technologies will be critical to the growth and market penetration of renewable energy sources such as solar and wind [1-3]. Electrochemical capacitors (ECs) or supercapacitors have attracted increased attention for their applications in energy storage due to their high power density, rapid charge-discharge capability, and long cycle life [4-7]. Supercapacitors can store energy through two primary mechanisms: electrochemical double layer capacitance (EDLC) involving physical adsorption of ions from the electrolyte and pseudocapacitance involving reversible Faradaic redox reactions [8]. Currently, nearly all commercial supercapacitors are EDLCs due to their relatively low material cost and outstanding durability, exceeding 100,000 cycles [9-11]. Reaching high capacitance by charging the double layer requires electronically conducting electrodes with high specific surface area. Carbon materials, with their high conductivity, electrochemical stability, and open porosity are excellent candidates for EDLC electrodes [1]. Numerous carbon allotropes have been explored for supercapacitor applications including activated, templated, and carbide derived carbon [12], as well as carbon nanotubes [13], graphene [14], and carbon onions [15]. Activated carbon, however, remains the most common material used for EC electrodes owing to its high specific surface area and low cost.

The microstructure present within activated carbon strongly affects its capacitive performance due to the influence of porosity on ion mobility within the carbon structure. Although, mesoporosity in the 2-50 nm range is considered ideal for ion mobility and thus desirable for superior energy and power density, several recent studies have demonstrated important capacitive contributions from micropores [1, 16-18]. Micropores smaller than 1 nm have been shown to provide enhanced capacitive effects in both aqueous and organic electrolytes [19-21]. This phenomenon has been attributed to partial desolvation of the electrolyte ions, allowing for access to small micropores and a closer approach to the carbon surface [22]. In addition to the porosity of activated carbon, its surface chemistry can also play an important role in its capacitive properties. For instance, the presence of functional groups on the carbon surface can increase wettability in aqueous electrolytes improving the utilization of the specific surface area [23]. More importantly, oxygen and nitrogen functionalities can participate in faradic redox reactions increasing the energy storage of carbon through pseudocapacitance. Thus, highly porous and highly functionalized activated carbon has been shown to demonstrate both high specific capacitance and energy density [24-26].

Although porosity and surface chemistry are important

characteristics for the capacitive performance of carbon electrodes, other factors such as material cost and environmental impact are critical when considering potential commercial applications. For large scale renewable energy storage, engineering electrodes which utilize waste materials from nature has great potential for overcoming environmental and cost constraints. Biochar activated carbon, produced from the pyrolysis of inexpensive biomass feedstock (wood, manure, agricultural residue) has attracted attention for supercapacitor electrode applications [23, 27-30]. Since the majority of biomass sources are renewable agricultural waste products, biochar carbon can be produced sustainably at a promisingly low cost. As a result, there have been numerous recent reports of biochar-based supercapacitor electrodes. For instance, activated carbon prepared from cotton stocks demonstrated a capacitance of 114 F g^{-1} [30], while sawdust physically activated with a CO_2 stream showed a capacitance of 134 F g^{-1} [31]. High specific surface area carbon (>2000 m^2 g^{-1}) demonstrating capacitance over 300 F g^{-1} was produced from sunflower seed shells with the aid of KOH impregnation [32]. Biochar derived from corn grains [33-34] and various woody precursors [35-36] have been reported with specific capacitance in the 100-250 F g^{-1} range depending on the activation conditions. Although the specific capacitance values reported above are quite high, many of these materials require complex or lengthy synthesis procedures (often involving addition chemical agents such as $ZnCl_2$, H_3PO_4, or KOH). Furthermore, many of the activated biochar electrodes demonstrated limited capability for high rate charge-discharge (a common performance limitation for activated carbon). This poor capacitance retention at high rates can be attributed to the disordered graphitic structure and large micrometer particle size present in many activated carbon materials which results in poor electronic and ionic conductivity. These properties differ greatly from those of highly ordered "open" 2D structures like graphene which show excellent electronic conductivity and short ion diffusion distances [37].

In the ideal case one could combine the low cost and sustainability of biomass activated carbon with the excellent performance characteristics of nanomaterials like graphene. Thus, recent efforts have focused on using biomass precursors to produce porous activated carbon with 2D nanostructures. For instance, high performance carbon materials displaying graphene-like nanosheets have been successfully synthesized from coconut shells [38], corn stalks [39], and hemp bast fibers [40]. The synthesis of these nanomaterials from biomass precursors requires a tailored synthesis strategy often involving activation agents or biomass pre-treatment steps [37].

In this work we aim to use corn cob as an inexpensive biomass precursor for scalable production of a high performance biochar material with a porous nanosheet structure. Corn is one of major crops in the world. Dust-free corn cob can be obtained at very low cost and very large scale after corn harvest. Moreover, corn cob has high carbon content (>40 wt%), heterogeneous porous microstructures, and very low trace-element content (<1.5 wt%). These attributes enable corn cob to be a highly desirable biomass feedstock for cost-effective production of nanostructured biochar. The biochar synthesis route developed in this work first involved a dilute acid biomass pre-treatment aimed at enriching the corn cob precursor in its crystalline cellulose component to better expose the inherent nanoarchitectures. This pre-treatment step was combined with a novel post pyrolysis thermal-chemical flash procedure to exfoliate the biochar and reveal porous carbon nanosheets. The structure and composition of this material were fully characterized and its potential application as an energy storage material for supercapacitor electrodes was investigated. The efficacy of the tailored synthesis route was evaluated through comparison to natural corn cob biochar produced without pre-or post-treatment modifications.

Experimental Section

Preparation of biochar carbon

Clean corn cobs used in this investigation were collected from a corn field close to the Urbana-Champaign area in Illinois, U.S.A, after kernels were removed from the corn ears. Typically, the corn cobs with red beeswing appearance (Figure S1) contain 44.0% carbon, 7.0% hydrogen, 47.0% oxygen, 0.4% nitrogen and 1.5% trace elements. In this study, the central soft pith part of the cob was removed for future analysis, leaving behind the hard outer woody ring which comprises the majority of the cob. In a typical synthesis of the *natural biochar* material, corn cob shells (2-4 g), without further treatment, were pyrolyzed in a tubular furnace at 900°C for 2 hours with a heating rate of 5°C min^{-1} in a nitrogen atmosphere. For the exfoliated biochar carbon, the corn cob shells (2g) were crushed into 5-10 mm chunks and soaked in 1M HNO_3 (20ml) at 75°C for 4 hours in a dilute acid pre-treatment step. The pretreated corn cob material was recovered by filtration, dried, and pyrolyzed under the same conditions as the natural material. This was followed by oxidation in conc. HNO_3 for at least 4 hours. The oxidized carbon was thermally exfoliated via a 45 second flash heat treatment in a high temperature muffle furnace. Four different flash temperatures were evaluated: 450°C, 750°C, 950°C, and 1050°C. The results are reported for the optimal flash temperature of 950°C, chosen based on the electrochemical performance of the material. This pretreated and thermally flashed material is referred to as *exfoliated biochar*. The preparation conditions for both the natural and exfoliated material are summarized in Table 1.

Table 1 Preparation Conditions for natural and exfoliated biochar material

Sample	Pre-treatment	Pyrolysis	Post-treatment
Natural biochar	--	900°C for 2 hours in N_2 atmosphere	--
Exfoliated biochar	1M HNO_3 for 4 h at 75°C	900°C for 2 hours in N_2 atmosphere	HNO_3 oxidation and thermal flash (45 s at 950 °C)

Physical and Chemical Characterization

The non-destructive 3-dimensional characterization of pore microstructures was performed using a high-resolution 3D X-ray imaging system MicroXCT-200 with sub-1 micron pixel resolution. Raman measurements were performed using a high-resolution research-grade Horiba LabRAM HR 3D-capable Raman spectroscopy imaging system with a 532nm wavelength laser source. The surface morphology of the samples was studied with a Philips XL30 ESEM-FEG field emission environmental scanning electron microscope (ESEM) operating at 15kV as well as a Philips CM200 Transmission Electron Microscope (TEM) operating at 200 kV. Surface area and porosity were investigated using nitrogen adsorption at 77K (Micrometrics ASAP 2020 Physisorption Analyzer). The surface chemistry of the carbon materials was analyzed with X-ray Photoelectron Spectroscopy (XPS) and Fourier Transform Infrared Spectroscopy (FTIR). XPS measurements were conducted using a Leybold Max 200 X-ray photoelectron spectroscope with a monochromatic aluminum (Al) Kα X-ray source. All XPS spectra were calibrated with respect to the C1s peak at 284.6 eV. FTIR spectra were collected using a Thermo Nicolet Nexus 670 FTIR spectrometer using KBr wafers containing approximately 25-50 mg of carbon powder.

Electrode Preparation and Electrochemical Measurements

The working electrodes used for tests in the 3 electrode cell configuration were prepared by cutting chunks of the biochar material into small monoliths weighing approximately 1 mg. These small monoliths were wrapped in gold wire and used directly as the working electrode without introducing any organic binder, which facilitated the fast evaluation of the intrinsic electrochemical properties of biochar materials under varying conditions. Tests in the three electrode configuration were performed using a 0.5 M H_2SO_4 electrolyte, Pt mesh counter electrode, and Ag/AgCl reference electrode. For evaluation of the symmetric 2 electrode supercapacitor device, biochar electrodes were prepared by combining biochar carbon (90 wt. %) with Nafion binder (10 wt. %) in an aqueous ink, which was then coated on titanium foils and dried at 80°C for 1 hour. Two similar electrodes with mass loadings of approximately 1.5 mg cm^{-2} were separated by glassy filter paper in a 0.5 M H_2SO_4 electrolyte. Cyclic voltammetry (CV) and galvanostatic charge-discharge cycling were performed using an Autolab general purpose electrochemical instrument PGSTAT30 (Metrohm, USA). In the 3 electrode configuration, the specific capacitance (C) of the biochar electrode was calculated from the charge-discharge curve according to:

$$C = \frac{I\Delta t}{m_m \Delta V} \quad (1)$$

where I is the charge-discharge current, t is the discharge time, m_m is the mass of the biochar monolith, and ΔV is the potential window. In the symmetric device configuration, the evaluation of the carbon electrode capacitance from the charge-discharge curve is modified slightly as follows:

$$C = \frac{2I\Delta t}{m_e \Delta V} \quad (2)$$

where m_e corresponds to the mass of the biochar active material on a single electrode. The durability of the biochar electrodes was evaluated in the symmetric device configuration by applying 5000 successive CV cycles.

Electrochemical Impedance Spectroscopy (EIS) measurements were also carried out using the Autolab PGSTAT30. The frequency range studied was 10 kHz to 10 mHz and all measurements were made at the rest potential of the cell. The real $C'(\omega)$ and imaginary $C''(\omega)$ portions of the capacitance were calculated from the EIS data according to the following equations [41]:

$$C'(\omega) = \frac{-Z''(\omega)}{\omega |Z(\omega)|^2} \quad (3)$$

$$C''(\omega) = \frac{Z'(\omega)}{\omega |Z(\omega)|^2} \quad (4)$$

Z' and Z'' are the real and imaginary portions of the electrochemical impedance (Z) respectively, and ω is the frequency in radians. The time constant for the symmetric EC device was calculated based on the frequency at which the plot of imaginary capacitance reaches a maximum [41].

Results and Discussion

Synthesis Strategy for Corn Cob Biochar Carbon

The corn cob feedstock used in this work is comprised mainly of crystalline cellulose dispersed in other amorphous plant phases such as hemicellulose and lignin [42]. The crystalline cellulose polymers are contained in densely packed nanosheet stacks which are surrounded by the amorphous components [43]. The goal of this work is to isolate and carbonize the crystalline cellulose fraction, and exfoliate this material to reveal the inherent nanostructure, producing a high surface area carbon product. The synthesis strategy depicted in Fig. 1 consists of biomass pre-treatment to remove the amorphous surroundings, pyrolyis in a N_2 atmosphere to carbonize the cellulose nanosheets, and combined thermal-chemical flash to exfoliate the stacks and simultaneously introduce functional groups to carbonized surfaces. The corn cob feedstock was first subjected to dilute acid pre-treatment to preferentially hydrolyze the hemicellulose and lignin to enrich the precursor in crystalline cellulose. After this pretreated material was pyrolyzed, the resulting biochar product was thermally exfoliated. Thermal exfoliation has been used extensively in the production of graphene sheets from graphite oxide [44-45]; however in this investigation a more powerful procedure is adapted in an effort to exfoliate a biochar carbon substrate. The exfoliation process involved the incorporation of strong oxidative nitric acid followed by a high temperature flash treatment at 950°C for 45 seconds in an air atmosphere. The high temperature flash will result in explosive decomposition of the incorporated acid and surface oxides, the force of which helps to exfoliate the carbon nanosheet stacks into thinner nanosheets with surfaces accessible to gas or liquids. The acid and its decomposition products have the ability to oxidize the carbon surfaces at this temperature, leading to the formation of strongly bound surface oxygen and the consumption of some of the carbon backbone, thus the sheet-like structures developed demonstrate considerable porosity. The physical and chemical properties of exfoliated biochar as well as its electrochemical performance are

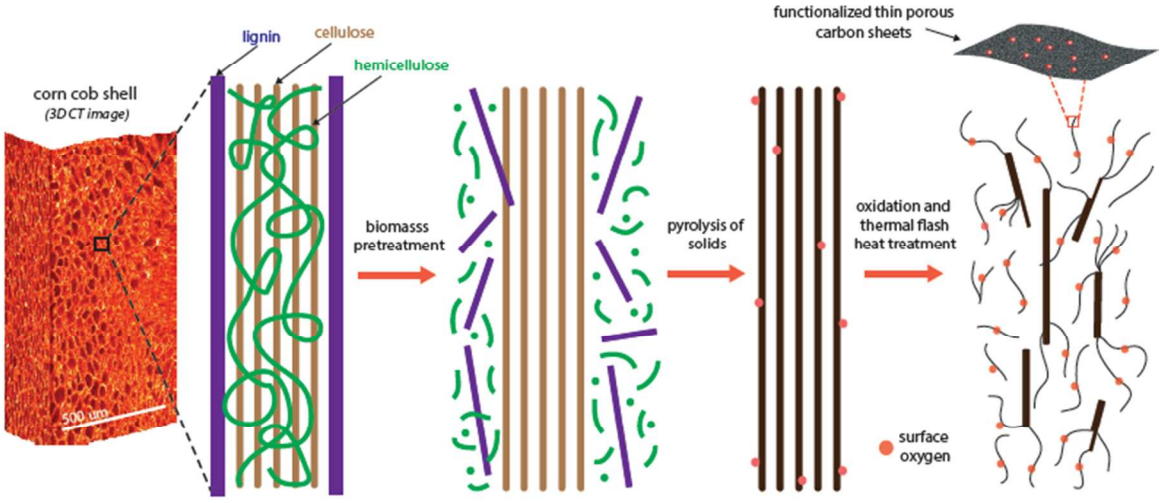

Fig. 1 Schematic representation of the synthesis strategy for the exfoliated corn cob biochar

in the following evaluated and compared with natural biochar material prepared without pre- or post-pyrolysis modification.

Molecular Structure and Surface Morphology

Raman spectroscopy is an excellent tool for analyzing carbon materials as their Raman spectra have been shown to be sensitive to changes in the microscopic structure of the material [46]. The Raman spectra of both the natural and exfoliated biochar carbon materials (Fig. 2A) both demonstrated the characteristic D and G peaks observed at 1350 cm^{-1} and 1575cm^{-1} respectively. The G band corresponds to the allowed Raman transition for large graphite crystals and is thus indicative of graphitic layers, while the D band corresponds to disordered carbon or defective graphitic structures [46-47]. The relative intensity of the G and D bands (I_G/I_D), as calculated by the peak area, can be used as an indication of the molecular order within the crystalline carbon structure and has been related to the size of the graphite crystallite [46]. The natural corn biochar demonstrates an I_G/I_D ratio of 0.68, while the spectrum of the exfoliated sample showed a significant reduction in the full width half maximum (FWHM) of the D band resulting in a much larger I_G/I_D of 0.89. This indicates a more ordered crystalline carbon structure in the exfoliated material, which is most likely a result of the pre-treatment step which preferentially removed the amorphous hemicellulose and lignin components. The spectra of both samples also show the 2D Raman feature at 2750 cm^{-1}. For the exfoliated material, this band has separated into two more narrow and defined peaks as opposed to the single broad feature shown by the natural material. A narrower and better defined 2D feature is another indication of increased crystalline order within a carbon material [46].

While the pre-treatment portion of the synthesis strategy appeared to be effective in enriching the crystalline component of the material, the efficacy of the thermal-chemical flash post treatment in exfoliating the carbon structure was examined through Scanning Electron Microscopy (SEM) and Transmission Electron Microscopy (TEM) analyses. Fig. 2B shows a SEM micrograph of the natural corn cob biochar material which demonstrates an ordered honey-comb structure of macropores measuring 10-20 μm in diameter, separated by relatively thick (1-

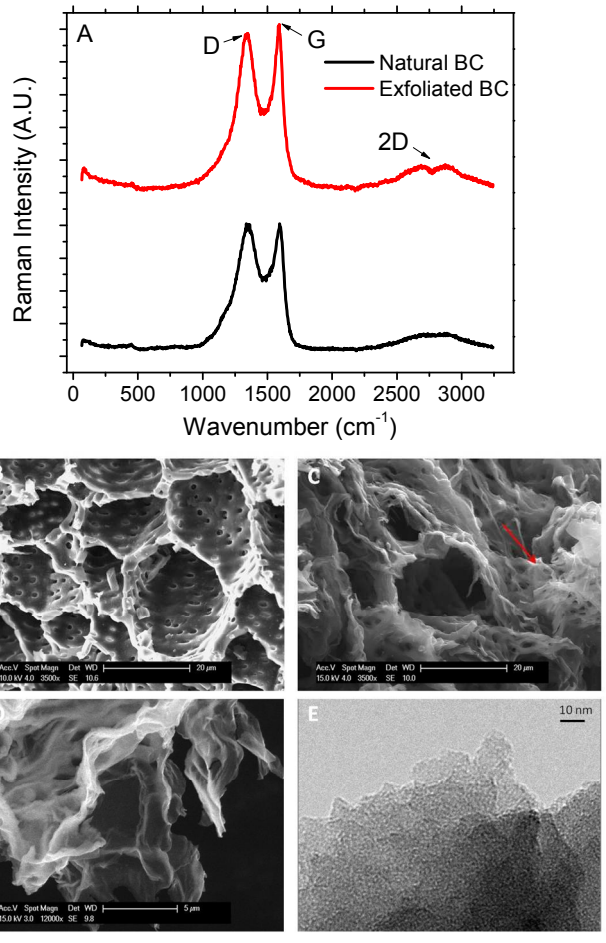

Fig 2. Raman spectra of natural and exfoliated biochar (BC) carbon (A). SEM images of the natural (B) and exfoliated (C, D) biochar illustrating the change in surface morphology after the exfoliation procedure. TEM image of the exfoliated material (E) depicting a layered structure of thin microporous nanosheets

3 μm) pore walls. However, the morphology of the exfoliated carbon sample (Fig. 2C) is very different; the combination of the pre-treatment and flash has frayed and shredded the thick pore walls revealing thin sheet-like carbon architectures. The ordered network of honeycomb macropores has been transformed into an array of layered carbon sheets. The biochar material is not completely exfoliated as remnants of the original structure remain and portions of the carbon sheets are still relatively thick. However, in many areas, such as the one highlighted in Fig. 2C (red arrow), the effect of the flash in exfoliating the biochar structure is profound. The material appears as a "fluffy" agglomeration of thin carbon sheets, similar to morphologies reported in SEM studies of dry graphene powder [44]. Fig. 2D shows a higher resolution image of the exfoliated material, providing a clear indication of these thin sheet-like carbon structures which starkly contrast with the thick walled honeycomb morphology of the natural material. The importance of both the pre and post pyrolysis treatments to this exfoliation process is demonstrated in Fig. S2(B), which shows an SEM micrograph of a biochar sample subjected to the flash post treatment, but no biomass pretreatment. In this case, the flash post treatment only slightly disrupts the structure of the natural biochar with tightly stacked carbon layers becoming partially visible. However, with the amorphous surrounding removed via pretreatment, the thermal-chemical flash can exfoliate these stacked layers more effectively to reveal thin carbon sheets.

The structure of the exfoliated biochar was explored further with high resolution TEM imaging (Fig. 2E), which reveals a thin layered structure of carbon nanosheets. The layered nanosheet structures are highly porous and become progressively thinner toward the edges of the material. The white spots distributed in gray areas correspond to the pores. The sheets appear to be predominately microporous with most pores measuring between 0.5 and 2.0 nm in diameter. These highly porous nanosheets are most likely a result of the thermal-chemical flash exfoliation. In addition to exfoliating the carbon surface and revealing sheet-like structures, the formation of CO or CO_2 through oxidative consumption of the carbon backbone during the high temperature flash is likely to increase the porosity of the exfoliated sheets.

Porosity and Chemical Composition

Analyses of the biochar morphology via SEM and TEM provided a qualitative indication of increased porosity due to the exfoliation procedure. To quantify the true effect of the exfoliation on the surface area and porosity of the material, nitrogen adsorption analysis was employed. Table 2 provides a summary of the textural characteristics of both the natural and exfoliated biochar materials. The natural corn cob biochar material demonstrated a BET specific surface area of only 7.9 m^2 g^{-1}. A very low specific surface area is common for untreated corn cobs pyrolyzed at high temperature and has been reported by Romanos et al. [48]. With exfoliation, however, the surface area of the corn biochar increases dramatically to 543.7 m^2 g^{-1}. The microporous surface area of the exfoliated material, calculated via the *t plot* method, was found to be 540.0 m^2 g^{-1}, consistent with TEM analysis, which suggested that the exfoliated biochar is predominately microporous. Similarly, the nitrogen adsorption isotherm of the exfoliated material (Fig. S3) demonstrated the Type I behaviour indicative of a strong microporous contribution. In order to evaluate the pore volume and size distribution of the micropores, the Horvath-Kawazoe method assuming slit pore geometry was used with the results shown in Fig. 3. The exfoliated material demonstrates a significant increase in pore volume over the natural biochar with a sharp peak and narrow size distribution around 0.6-0.7 nm as well as a broad humplocated at 1.1-1.7 nm. This increase in pore volume can be attributed to both the porosity created directly during the flash and the intrinsic porosity of the material revealed through exfoliation. It has been suggested that the microporous nature of the exfoliated material could be valuable for double layer capacitive applications as sub nanometer pores have been shown to demonstrate an enhanced capacitive effect [19-21]. XPS was used to evaluate the surface chemical composition of

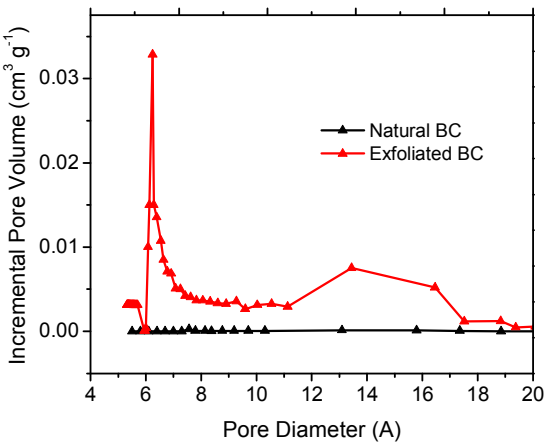

Fig. 3: Pore size distribution of natural and exfoliated biochar (BC) samples calculated by the Horvath-Kawazoe method

Table 2 Physical and chemical properties of natural and exfoliated biochar samples

	S_{BET} [m^2 g^{-1}]	$S_{t\text{-}plot}$ [a] [m^2 g^{-1}]	V_T [cm^3 g^{-1}]	XPS [b]			I_G/I_D [c]	C_g [d] [F g^{-1}]
				C %	O %	N %		
Natural BC	7.91	5.24	0.0018	97.5	1.9	0.6	0.68	221.3
Exfoliated BC	543.68	539.98	0.25	90.3	8.5	1.2	0.89	2.1

[a] Microporous surface area calculated by the t-plot method. [b] Atomic percentage of C, O, and N determined from XPS analysis. [c] Area Ratio of G and D bands from Raman spectra. [d] Capacitance at current density of 0.5 A g^{-1} in 0.5 M H_2SO_4.

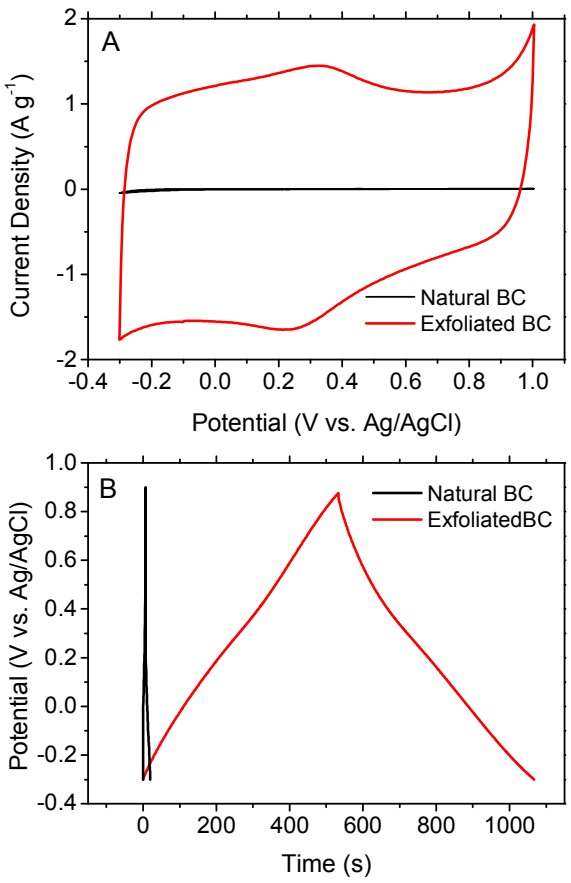

Fig. 4 Electrochemical performance of the natural and exfoliated biochar (BC) electrodes in a 3-electrode cell with 0.5 M H_2SO_4 electrolyte. Cyclic voltammograms at 5 mV s^{-1} (A); galvanostatic charge-discharge curves at 0.5 A g^{-1}(B)

the natural and exfoliated biochar materials with the atomic percentage of the surface elements summarized in Table 2. The natural corn biochar showed very high carbon content of 97.5 % with only 1.9 % surface oxygen and 0.6 % surface nitrogen. The exfoliated biochar, however, showed a slight increase in nitrogen content to 1.2 % but a more dramatic increase in surface oxygen to 8.5 %. These results suggest that the exfoliated material has a much higher concentration of oxygen surface functional groups. This increased oxygen content is likely a result of the high temperature flash treatment. Prior to the flash, the biochar carbon is oxidized with a strong acid and, as discussed, there could be partial desorption of surface oxides during the high temperature treatment. However, the simultaneous high temperature chemical oxidation of the carbon surface is likely to create more stable surface oxygen groups. This is supported by the XPS results which indicate that a significant amount of oxygen remains bound to the surface of the exfoliated sample. Therefore, in addition to exfoliating the biochar, the flash treatment is also effective in functionalizing the carbon surface.

Electrochemistry of Biochar Electrodes

In order to explore the potential application of the corn cob biochar material as an electrode for supercapacitors, the electrochemical and capacitive properties were evaluated using a 3 electrode configuration in 0.5 M H_2SO_4. The cyclic voltammograms of both the natural and exfoliated biochar at a scan rate of 5 mV s^{-1} are shown in Fig. 4A. The measured current density of the natural carbon material was quite low, resulting in a specific capacitance of only 2.1 F g^{-1}. The low capacitance of the natural material is not surprising considering its limited specific surface area for double layer charge storage. The exfoliation treatment seemed to have a dramatic effect on the electrochemical performance of the carbon, as the CV of the treated material demonstrated current densities over 100 times greater than that of the natural biochar. The exfoliated material also showed excellent capacitive behavior as indicated by a close to ideal rectangular CV over the entire 1.3 V potential window.

The CV of the treated carbon demonstrated characteristic broad peaks located at approximately +0.3 V vs. Ag/AgCl, indicative of the Faradaic redox processes associated with carbon materials that possess high oxygen functionality [24, 49, 50]. The peak separation between the oxidation and reduction features was only about 50 mV indicating good electrode conductivity and reversible redox behavior of surface functional groups. The exfoliated material also demonstrated relatively high hydrogen overpotential: An incremental CV scan (Fig. S4) revealed that the potential window could be pushed to 1.6 V with no sign of significant hydrogen evolution.

The galvanostatic charge-discharge curves for the natural and exfoliated biochar at 0.5 A g^{-1} are shown in Fig 4B. The exfoliated material demonstrates the ideal linear voltage-time relation with a capacitance of 221 F g^{-1} at a 0.5 A g^{-1} rate. This dramatic increase in capacitance over the natural material can be partly attributed to the enhanced double layer capacitance resulting from the increased surface area and porosity of the exfoliated material. The small micropores in particular may play an important role in the capacitive behaviour of the exfoliated sample. Both Raymundo-Pinero et al. [19] and Chmiola et al. [22] have demonstrated that ultramicropores in the 0.6-0.8 nm range, where the exfoliated biochar shows a strong distribution, can lead to enhanced capacitive effects due to ion desolvation. Nevertheless, it is unlikely that enhanced double layer capacitance is the only factor in the improved performance of the treated biochar. Activated carbon is generally characterized by an electrochemical double layer capacitance of 10-25 μF cm^{-2} [8, 25, 51]. Taking the upper limit of this range, the double layer capacitance of the exfoliated material can be estimated to be 135 F g^{-1}, assuming 100% utilization of the 540 m^2 g^{-1} surface area. Since the actual capacitance of the exfoliated biochar is well over 200 F g^{-1}, a significant portion of this capacity must originate from a mechanism beyond EDLC. The most likely source of this additional capacitance is the pseudocapacitive contributions of the redox active oxygen functional groups that are selectively enriched on the surface of the exfoliated material.

Biochar Surface Functionalities

There are many potential oxygen functionalities which can exist on the surface of biochar carbon including carboxylic acid, phenol, carbonyl, qunione, pyrone, and their derivatives. These oxygen groups demonstrate varying electrochemical activity and will therefore contribute differently to the faradic redox processes occurring on the carbon surface. FTIR and XPS analyses were

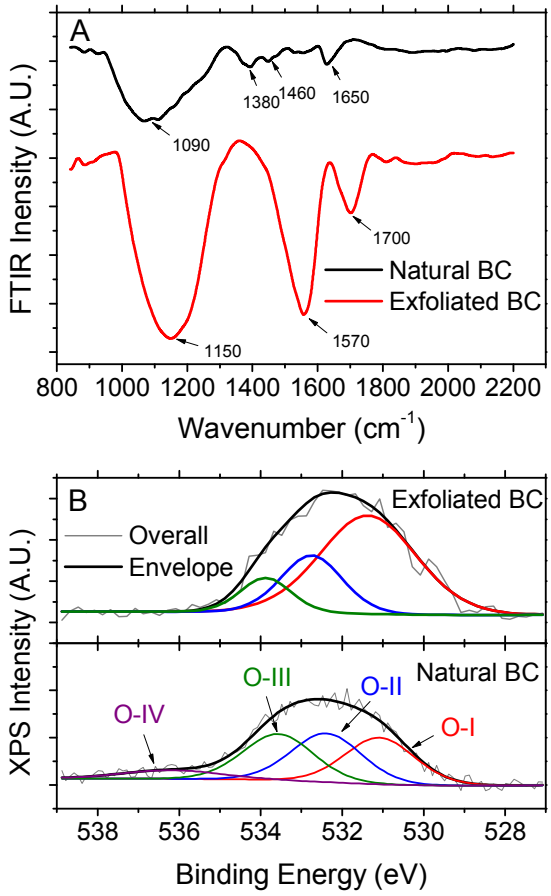

Fig.5 FTIR spectra (A) and XPS O1s spectra with deconvolution (B) for natural and exfoliated biochar (BC) samples

conducted to determine the nature of the biochar oxygen functionalities and their potential pseudocapacitive contribution. The effect of the exfoliation treatment on the oxygen functionality of the biochar is illustrated in the FTIR spectra (Fig 5A), while Table 3 summarizes the FTIR peak assignments. The spectrum of the natural material displays only one strong feature at 1090 cm^{-1}; however bands in this region (1200-1000 cm^{-1}) are difficult to assign as they are often composed of many broad superimposed peaks [52]. The remaining peaks in the natural biochar spectrum are quite small, including two features in the 1380-1460 cm^{-1} range which can be assigned to C=C deformation in phenols as well as O-H deformation in carboxylic acids [53-55]. There is also a small peak located at 1650 cm^{-1} which can be attributed to a C=O vibration of carboxylics and carbonyls [54]. The exfoliated biochar has quite a different FTIR spectrum demonstrating much larger peaks indicating increased oxygen functionality. The strong peak at 1570 cm^{-1} has been attributed to aromatic C=C stretching that is highly conjugated to carbonyl groups [53-55]. The feature at 1700 cm^{-1} can be assigned to C=O vibrations especially those present in aromatic rings as is the case for quinone and pyrone groups [54]. These results suggest that the surface of the exfoliated material may be enriched in these complex aromatic carbonyl functionalities.

High resolution XPS O1s analysis (Fig, 5B) was used to further examine the nature of the oxygen species on the biochar surface. The O1s band of both the natural and exfoliated material

Table 3 FTIR peak assignments for natural and exfoliated biochar

Wavenumber (cm-1)	Assignment	References
1380	C=C deformation in aromatic rings	[53, 55]
1460	O—H deformation in carboxyl groups	[53, 54]
1570	C=C stretching aromatics highly conjugated to carbonyl groups	[53-55]
1650	C=O vibration in carboxylic and carbonyl	[54]
1700	C=O stretching present in conjugated aromatics	[54]

was deconvoluted into three primary peaks: Peak O-I (531.1-531.3 eV) representing carbonyl oxygen; peak O-II (532.4-532.7 eV) representing carbonyl oxygen in carboxylics and anhydydes, as well as oxygen atoms in hydroxyl groups; and peak O-III (533.6-533.8 eV) representing non carbonyl (ether-type) oxygen in esters and anhydrides [56-57]. The natural material also demonstrated a fourth peak at high binding energy (536.1 eV) which was attributed to adsorbed water. The relative intensities of the contributing O1s peaks are summarized in Table 4. The natural biochar displays a broad O1s line with a relatively equal contribution from peaks O-I, O-II, and O-III. The exfoliated material, however, demonstrated a narrower O1s feature with the majority of the contribution (64.3%) stemming from carbonyl oxygen. Thus, the XPS data agrees with the findings in FTIR which indicated that carbonyl type groups such as quinone and pyrone are the predominant oxygen functionalities on the surface of the exfoliated biochar. These results can also help to explain the large pseudocapacitance contribution to the exfoliated biochar electrode highlighted in the previous section.

Quinone oxygen has been reported as one of the main sources of pseudocapacitance in activated carbon due to the quinione/hydroquinone redox reaction that is quite reversible [24, 58]. These reactions are characteristic of the redox humps located at +0.3 V vs. Ag/AgCl [24, 49] which were clearly demonstrated in the CV of the exfoliated biochar. Furthermore, pyrone functionalities can also contribute to pseudocapacitance and this redox activity can be located in a similar potential region as that of quinone or at even higher redox potentials in the case of complex pyrone configurations [49-50, 59]. Conversely, the strongly acidic carboxylic acid groups, which appear in higher proportion on the natural material, are generally considered to possess poor electrochemical activity and reversibility [23]. The

Table 4 Relative content of oxygen functional groups for natural and exfoliated biochar based on deconvolution of the XPS O1s spectra

	% Total of O1s			
	O-I	O-II	O-III	O-IV
	531.1-531.3 eV	532.4-532.7 eV	533.6-533.8 eV)	(536.1 eV)
Natural BC	30.3	33.7	30.2	5.8
Exfoliated BC	64.3	20.9	14.8	- -

increase in the proportion of the basic electrochemically active surface oxides on the exfoliated material can be attributed to the flash heat treatment. Basic oxygen containing species such as quinone and pyrone have been shown to have much higher thermal stability than acidic species such as hydroxyl or carboxylic acid [57, 61]. Therefore, at the high temperature of the flash treatment (950°C), oxygen that reacts and remains on the carbon surface will take the form of the surface species that are more stable at this high temperature (quinine and pyrone). Similar results were reported by both Papirer et al. [60] and Yoshida et al. [61] who found that oxidized carbon materials treated at 1000°C and exposed to an oxygen atmosphere showed a reduction in the surface concentration of carboxylic and phenolic species, and an increase in the concentration of quinone and pyrone species. The above results indicate that the flash not only helps to exfoliate the carbon and increases porosity, but also selectively enriches the carbon surface in redox active surface functionalities. This combined effect translates into increased double layer and pseudocapacitive contributions which explains the dramatically enhanced charge storage capacity demonstrated by the exfoliated biochar material.

Evaluation of Exfoliated Biochar Supercapacitors

The high degree of porosity and oxygen functionality of the exfoliated biochar material can be valuable for supercapacitor applications. The exfoliated sample was scaled up to 1cm^2 electrodes and tested in a symmetric two-electrode supercapacitor cell with a 0.5 M H_2SO_4 electrolyte. At a scan rate of 50 mV s^{-1}, the CV of the exfoliated material (Fig 6A) demonstrated a near ideal rectangular shape over a 1.0 V potential window. Even when the scan rate was increased, no significant distortion in the CV was observed (Fig. 6B). At the high rate of 500 mV s^{-1} the CV still maintained a quasi rectangular shape indicating fast ion transport and excellent overall electrode conductivity.

The capacitive performance of the exfoliated biochar was investigated by galvanostatic charge-discharge experiments. The exfoliated carbon material demonstrated a capacitance of 210 F g^{-1} at a 0.5 A g^{-1} rate; approximately 5% less than the value observed with the 3 electrode set-up. This type of reduction is common when an organic binder is used and when moving from a 3 electrode to 2 electrode cell configuration, especially in pseudocapacitive materials where the redox peaks may prevent perfect charge balancing between negative and positive electrodes. Nevertheless, the high capacitance demonstrated by the exfoliated biochar is comparable to carbon materials with much larger BET specific surface area [10, 62]; a direct result of the abundant redox active functionalities present on the exfoliated biochar surface. Figure 6C shows galvanostatic charge discharge curves for the exfoliated biochar over a range of current densities from 1 to 10 A g^{-1}. Even at 10 A g^{-1} the galvanostatic curve maintains the ideal linear voltage time relation, displaying minimal *I* R drop. The capacitance retention of the electrodes for rates up to 40 A g^{-1} is summarized in Figure 6D. The biochar supercapacitor demonstrates outstanding high rate performance, maintaining a capacitance of 165 F g^{-1} (78% of its low rate value) at a fast 40 A g^{-1} discharge. While the large specific capacitance of the exfoliated material is comparable to recent reports of other high performance nanostructured ACs [33, 38, 63]; the capability of the exfoliated BC electrode for high rate charge/discharge is

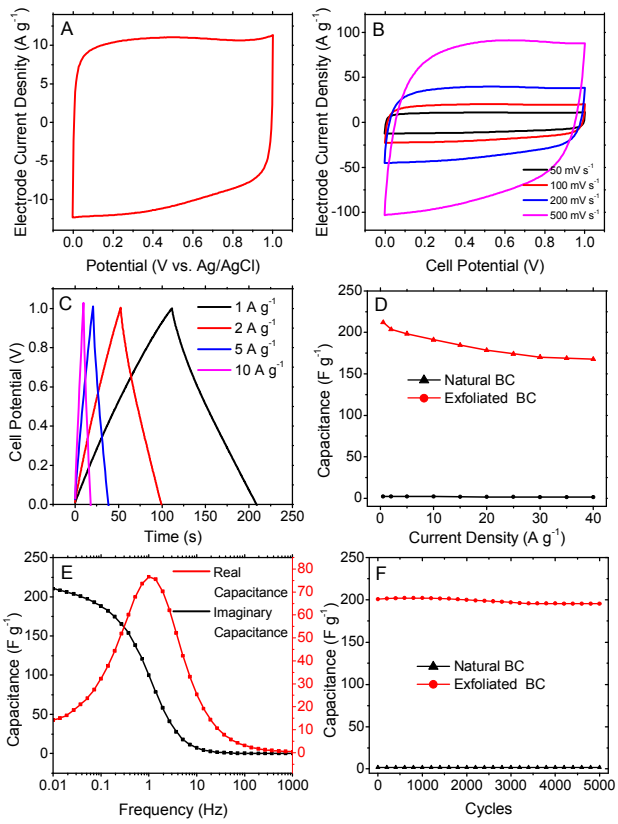

Fig. 6: Electrochemical performance of exfoliated biochar electrodes in a symmetric 2 electrode supercapacitor cell with 0.5 M H_2SO_4 electrolyte. Cyclic voltammogram at 50 mV s^{-1} (A); cyclic voltammograms at increasing rates from 50 to 500 mV s^{-1}(B); galvanostatic charge discharge at rates from 1 to 10 A g^{-1}(C); capacitance retention with increasing discharge rate (D); real and imaginary capacitance as a function of frequency (E), evolution of specific capacitance upon repeated potential cycling (F).

far superior. This combination of high capacitance and fast charge-discharge capability distinguishes the exfoliated biochar from most other porous activated carbons. In fact, the capacitive behaviour of the exfoliated BC is more comparable to that recently reported for designer nanomateirals such as hydrazine reduced graphene oxide [64] and CNT/graphene hybrids [65].

The rapid ion and electron transfer properties of the exfoliated material were further demonstrated by electrochemical impedance spectroscopy. Complex capacitance diagrams which plot the real and imaginary capacitance vs. frequency are illustrated in Fig. 6E. The frequency at which the plot of imaginary capacitance reaches a maximum defines a device time constant (τ=1/f). Smaller time constant values are indicative of superior capacitive performance brought about by fast ion and electron transfer behaviour. The exfoliated material demonstrated a time constant of 1s which is excellent when compared to other porous activated carbon materials with similar capacitance [41, 66]. Additionally, the real capacitance of 208 F g^{-1} measured at the low frequency of 10 mHz agreed nicely with the electrode capacitance determined from galvanostatic discharge. Durability tests also revealed that the exfoliated biochar electrode displays excellent cycling stability, suffering only a 3% reduction in capacitance after 5000 successive

potential cycles (Fig. 6F). The combination of high specific capacitance, excellent rate capability, and good cycle life suggest that the exfoliated corn cob biochar is a very promising material for high performance supercapacitor applications.

Conclusions

An abundant agricultural residue (corn cob) was used as a precursor to synthesize low cost biochar with a porous nanosheet structure for high performance supercapacitor electrodes. This exfoliated biochar material was produced via a tailored synthesis methodology involving dilute acid biomass pre-treatment and a novel post-pyrolysis thermal-chemical flash procedure. The exfoliated material showed increased graphitic order due primarily to the preferential removal of amorphous components before pyrolysis. Furthermore, the pre- and post-pyrolysis treatments dramatically affected the surface morphology of the material which was transformed from an ordered arrangement of honeycomb macropores in the natural biochar to an array of thin layered microporous nanosheets in the exfoliated material. The exfoliated biochar showed a BET surface area of 543.7 m^2 g^{-1}, far higher than the 7.9 m^2 g^{-1} of the natural material.

In addition to increasing the surface area and porosity of the material, the exfoliation procedure also added oxygen functionality to the carbon surface. This surface oxygen primarily took the form of electrochemically active quinone and pyrone type functional groups. The exfoliated biochar demonstrated a high specific capacitance of 221 F g^{-1}, over one hundred times larger than that of the natural biochar material. This substantial increase in charge storage after exfoliation resulted from the combined effect of increased surface area and oxygen functionality which led to enhanced double layer and pseudocapacitive contributions. The exfoliated biochar also demonstrated rate capability far superior to conventional activated carbon, retaining 78 % of its low rate capacitance at a fast 40 A g^{-1} discharge. Furthermore, the exfoliated electrodes proved to be quite durable showing minimal capacitance decay after 5000 successive potential cycles. It is very encouraging that this combination of high specific capacitance, durability, and excellent rate capability can be achieved from a carbon material based on an inexpensive waste feedstock. The combination of its low cost and demonstrated high performance suggest that the exfoliated corn cob biochar could be a very promising electrode material for energy storage applications. The exfoliation synthesis described in this work may be extended to the development of other high performance energy storage materials from a wide variety of biomass waste.

Acknowledgements

We acknowledge the financial support of NSERC Canada and Illinois Hazardous Waste Research Fund (USA). MG would like to thank the OGS program for a postgraduate scholarship and Hatch for a scholarship for sustainable energy research. We thank Dr. Leilei Yin at the Beckman Institute of Advanced Science and Technology of the University of Illinois at Urbana-Champaign for performing 3D X-ray computed tomography measurements.

Notes and references

[a] *Department of Materials Science and Engineering, University of Toronto, 184 College St. Toronto, ON M5S 3E4 Canada, Tel: 416-978-8631, E-mail: keryn.lian@utoronto.ca (Keryn Lian).*
[b] *Illinois Sustainable Technology Center, University of Illinois, Champaign, IL 61820, USA, Tel: 217-333-5550, Email: junhua@illinois.edu (Junhua Jiang).*

† Electronic Supplementary Information (ESI) available: [details of any supplementary information available should be included here]. See DOI: 10.1039/b000000x/

1 P. Simon, Y. Gogotsi, Nat. Mater. 2008, **7**, 845
2. H. Jiang, P. S. Lee, C. Z. Li, Energy Environ. Sci. 2013, **6**, 41.
3. C. Liu, F. Li, M. Lai-Peng, H. Cheng, Adv Mater, 2010, **22**, E28.
4. J. R. Miller and P. Simon, Science, 2008, **321**, 651.
5. J. Bae, M. K. Song, Y. J. Park, J. M. Kim, M. Liu and Z. L. Wang, Angew. Chem., Int. Ed., 2011, **50**, 1683.
6. S. Bose, T. Kuila, A.K. Mishra, R. Rajasekar, N.H. Kim and J.H. Lee, J. Mater. Chem., 2012, **22**, 767.
7. L. L. Zhang and X. S. Zhao, Chem. Soc. Rev., 2009, **38**, 2520.
8. B.E. Conway, Electrochemical Supercapacitor, Scientific Fundamentals and Technological Applications, Kluwer Academic, New York, 1999.
9. Z. Li, L. Zhang, B. S. Amirkhiz, X. H. Tan, Z. W. Xu, H. L. Wang, B. C. Olsen, C. M. B. Holt and D. Mitlin, Adv. Energy Mater., 2012, **2**, 431.
10. M. Sevilla and R. Mokaya, Energy Environ. Sci., 2014, **7**, 1250.
11. D. D. Zhou, Y. J. Du, Y. F. Song, Y. G. Wang, C. X. Wang and Y. Y. Xia, J. Mater. Chem. A, 2013, **1**, 1192.
12. T. Kyotani, J. Chmiola, and Y. Gogotsi, Carbon Materials for Electrochemical Energy Storage Systems: Ch. 13, CRC/Taylor and Francis, Florida, 2010.
13. Y.K. Hsu, Y.C. Chen, Y.G. Lin, L.C. Chen, and K.H. Chen, J. Mater. Chem., 2012, **22**, 3383.
14. Y. B. Tan and J.M. Lee, J. Mater. Chem. A, 2013, **1**, 14814.
15. C. Portet, J. Chmiola, Y. Gogotsi, S. Park, and K. Lian, Electrochim. Acta, 2008, **53**, 7675.
16. G. Salitra, A. Soffer, L. Eliad, Y. Cohen, and D. Aurbach, J. Electrochem. Soc. 200, **147**, 2486.
17. C. Vix-Guterl, E. Frackowiak, K. Jurewicz, M. Friebe, J. Parmentier, and F. Béguin, Carbon, 2005, **43**, 1293.
18. A. Janes, and E. Lust, J. Electrochem. Soc. 2006, **153**, A113.
19. E. Raymundo-Pinero, K. Kierzek, J. Machnikowski, and F. Beguin, Carbon, 2006, **44**, 2498.
20. M. Arulepp, J. Leis, M. Lätt, F. Miller, K. Rumma, E. Lust, and A.F. Burke, J. Power Sources, 2006, **162**, 1460.
21. J. Chmiola, R. Dash, G. Yushin, and Y. Gogotsi, J. Power Sources, 2006, **158**, 765.
22. J. Chmiola et al., Science, 2006, **313**, 1760.
23. J. Jiang, L. Zhang, X. Wang, N. Holm, K. Rajagopalana, F. Chen, and S. Mac, Electrochimica Acta, 2013, **113**, 481.
24. M. Seredych, D. Hulicova-Jurcakova, G. Qing Lu, and T. J. Bandosz, Carbon, 2008, **46**, 1475.
25. Z. Li, Z. Xu, X. Tan, H. Wang, C. M. B. Holt, T. Stephenson, B. C. Olsen and D. Mitlin, Energy Environ. Sci., 2013, **6**, 871.
26. Z. Li, Z. Xu, H. Wang, J. Ding, B. Zahiri, C. M. B. Holt, X. Tan and D. Mitlin, Energy Environ. Sci., 2014, **7**, 1708.
27. H. Jin, X. Wang, Z. Gu, J. Polin, Journal of Power Sources, 2013, **236**, 285
28. K. Kuratani, K. Okuno, T. Iwaki, M. Kato, N. Takeichi, T. Miyuki, M. Majima, and T. Sakai, J. Power Sources, 2011, **196**, 10788.
29. R. Frama, M. Deraman, A. Awitdrus, I. Talib, R. Omar, J. Manjunatha, M. Ishak,N. Basri, and B. Dolah, Int. J. Electrochem. Sci., 2013, **8**, 2547.
30. M. Chen, X. Kang, T. Wumair, J. Dou, B. Gao, Y. Han, G. Xu, Z. Liu, and L. Zhang, J. Solid State Electrochem., 2013, **17**, 1005.
31. E. Taer, M. Deraman, I. Talib, A. Awitdrus, S. Hashimi, and A. Umar, J. Electrochem. Sci., 2011, **1**, 3301.

32. X. Li, W. Xing, S.P. Zhuo, J. Zhou, F. Li, S.Z. Qiao, and G.Q. Lu, Bioresour. Technol., 2011, **102**, 1118.
33. M.S. Balathanigaimani, W.G. Shim, M.J. Lee, C. Kim, J.W. Lee, and H. Moon, Electrochem. Commun., 2008, **10**, 868.
34. Q.Q. Li, F. Liu, L. Zhang, B.J. Nelson, S.H. Zhang, C. Ma, X.Y. Tao, J.P. Cheng, and X.B. Zhang, J. Power Sources, 2012, **207**, 199.
35. M. Liu, L. Kong, P. Zhang, Y. Luo, and L. Kang, Electrochim. Acta, 2012, **60**, 443.
36. E. Ito, S. Mozia, M. Okuda, T. Nakano, M. Toyoda, and M. Inagaki, New Carbon Mater., 2007, **22**, 321.
37. H. Wang, Z. Li, and D. Mitlin, ChemElectroChem, 2014, 1, 332.
38. L. Sun, C. G. Tian, M. T. Li, X. Y. Meng, L. Wang, R. H. Wang, J. Yin, H. and G. Fu, J. Mater. Chem. A, 2013, **1**, 6462.
39. L. Wang, G. Mu, C. G. Tian, L. Sun, W. Zhou, P. Yu, J. Yin, and H. G. Fu, ChemSusChem, 2013, **6**, 880.
40. H. Wang, Z. W. Xu, A. Kohandehghan, Z. Li, K. Cui, X. H. Tan, T. J. Stephenson, C. K. Kingondu, C. M. B. Holt, B. C. Olsen, J. K. Tak, D. Harfield, A. O. Anyia, and D. Mitlin, ACS Nano 2013, **7**, 5131.
41. P. L. Taberna, P. Simon, and J. F. Fauvarque, J. Electrochem. Soc., 2003, **150**, A292.
42. R. Kumar, G. Mago, V. Balan, and C. E. Wymand, Bioresource Technology, 2009, **100**, 3948.
43. P. Kumar, D. M. Barrett, M. J. Delwiche, and P. StroeveInd. Eng. Chem. Res., 2009, **48**, 3713.
44. H. C. Schniepp, J.L. Li, M. J. McAllister, H. Sai, M. Herrera-Alonso, D. H. Adamson, R. K. Prudhomme, R. Car, D. A. Saville, and I. A. Aksay, J. Phys. Chem. B, 2006, **110**, 8535.
45. M. J. McAllister, J.L. Li, D. H. Adamson, H. C. Schniepp, A. A. Abdala, J. Liu, M. Herrera-Alonso, D. L. Milius, R. Car, R.K. Prudhomme, and I. A. Aksay, Chem. Mater., 2007, **19**, 4396.
46. R. Escribano, J.J. Sloan, N. Siddique, N. Sze, and T. Dudev, Vibrational Spectroscopy, 2001, **26**, 179
47. M. S. Dresselhaus, G. Dresselhaus, R. Saito, and A. Jorio, Phys. Rep., 2005, **409**, 47.
48. J. Romanos, M. Beckner, T. Rash1, L. Firlej B. Kuchta, P. Yu, G. Suppes, C. Wexler, and P. Pfeifer, Nanotechnology, 2012, **23**, 015401.
49. H. A. Andreas and B. E. Conway, Electrochimica Acta, 2006, **51**, 6510.
50. E. Raymundo-Piñero, F. Leroux, and F. Béguin, Adv. Mater., 2006, **18**, 1877.
51. B. Kastening, W. Schiel, and M Henschel, J. Electroanal. Chem., 1985, **191**, 311.
52. P. Painter, M. Starsinic, M. Coleman, Determination of Functional Groups in Coal by Fourier Tranform Infrared Spectroscopy: In Fourier Transform Infrared Spectroscopy, Academic Press, New York, 1985.
53. C. Moreno-Castillaa, M.V. Lopez-Ramon, and F. Carrasco-Marına, Carbon, 2000, **38**, 1995.
54. E. Fuente, J. A. Menendez, M. A. Dıez, D. Suarez, and M. A. Montes-Moran, J. Phys. Chem. B, 2003, **107**, 6350.
55. J. Zawadzski, Infrared spectroscopy in surface chemistry of carbons, Chemistry and Physics of Carbon, vol 21, Dekker, New York, 1989.
56. J. H. Zhou, Z. J. Sui, J. Zhu, P. Li, D. Chen, Y. C. Dai, and W. K. Yuan, Carbon, 2007, **45**, 785.
57. P. V. Lakshminarayanan, H. Toghiani, and C. U. Pittman Jr., Carbon, 2004, 42, 2433
58. C.T. Hsieh and H. Teng, Carbon, 2002, **40**, 667.
59. M.A. Montes-Moran, D. Suarez, J.A. Menendez, and E. Fuente, Carbon, 2004, **42**, 1219.
60. E. Papirer, S. Li and J. B. Donnet, Carbon, 1987, **25**, 243.
61. A. Yoshida, I. Tanahashi and A. Nishino, Carbon, 1990, **28**, 611.
62. J. Zhang and X. S. Zhao, ChemSusChem, 2012, **5**, 818.
63. B Xu, S Hou, H Duan, G Cao, M Chu, and Y Yang, J. Power Sources, 2013, **228**, 193.
64. K. Zhang, L. Mao, L.L. Zhang, H.S.O. Chan, X.S. Zhao, and J. Wu, J. Mat. Chem. A, 2011, **21**, 7302.
65. D. Yu and L. Dai, J. Phys. Chem. Lett., 2010, **1**, 467.
66. K. Kierzek , E. Frackowiak , G. Lota , G. Gryglewicz , and J. Machnikowski, Electrochimica Acta, 2004, **49**, 515.

TOC Entry

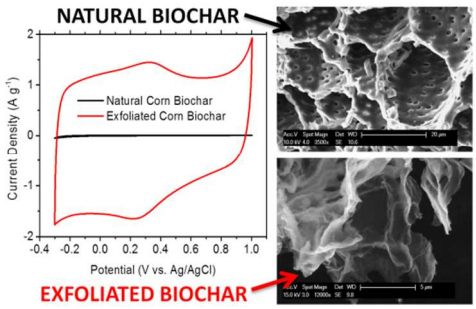

High performance biochar carbon nanosheets for supercapacitors are synthesized from corn cob waste via a novel exfoliation approach.